Theoretical investigation of DFSI with immunity to both Doppler effect and frequency-sweep nonlinearity[*]

ZHENG Feiteng[1,†], SHAO Bin[1,†,], SUN Shufeng[1,2], ZHANG Wu[1], TAN Qinggui[1], and ZHANG Wei[3,4]**

1. China Academy of Space Technology (Xi'an), Xi'an 710110, China

2. School of Electronic Information, Northwestern Polytechnical University, Xi'an 710129, China

3. The Key Laboratory of Optoelectronic Technology & Systems (Ministry of Education), Chongqing University, Chongqing 400044, China

4. Artificial Intelligence Center, Peng Cheng Laboratory, Shenzhen 518000, China

Frequency-swept interferometry (FSI) is a well-known ranging technique, but it suffers from three problems, namely, the Doppler effect, the frequency-sweep nonlinearity, as well as the slow frequency-sweep rate. The first two problems hinder the measurement accuracy, while the third problem limits the measurement rate. In this paper, we present a dynamic FSI (DFSI) that solves these three fundamental problems simultaneously. The DFSI consists of two auxiliary interferometers (AU1 and AU2) and two measurement interferometers (FSI and frequency-fixed interferometry (FFI)). We use FSI to obtain the Doppler and nonlinearity affected ranging signal, AU1 to monitor the frequency-tuning nonlinearity in the frequency-swept laser (FSL), and FFI and AU2 to constitute a laser vibrometer for monitoring the target motion-induced Doppler effect. Then, a novel signal fusion processing technique is applied to reconstruct the real dynamic distance from the above-measured signals. The dynamic ranging error caused by the Doppler effect and frequency-sweep nonlinearity in FSI can be eliminated and the dynamic distance at each sampling point can be obtained. The validity of this method is demonstrated by numerical experiments.

The basic frequency-swept interferometry (FSI) is merely suitable for static ranging. Once used for dynamic ranging, it becomes invalid. This is because on one hand, the basic FSI gives only one ranging value per sweep thus unable to adapt to high speed dynamic targets, and on the other hand, the ranging accuracy of basic FSI is severely deteriorated by the following two inevitable problems. One is the target-motion-induced Doppler effect. For FSI, if the target moves, the optical path difference (OPD) will vary during the frequency sweep period, and the Doppler error equals $\Delta L f_{avg}/B$, where f_{avg} and B are the average frequency and bandwidth of the frequency-swept laser (FSL), and ΔL is the distance change in a sweep cycle. f_{avg}/B usually ranges from hundreds to thousands, which means the Doppler error will be hundreds, even thousands, of times larger than the actual OPD variation[1-3]. To remove this error, a variety of methods have been reported[1-5]. These methods can effectively eliminate the Doppler error, while lacking the

immunity to the other problem, i.e., the frequency sweep nonlinearity. Specifically, due to the creep and hysteresis of the piezoelectric transducer inside the external cavity diode laser, the output laser frequency exhibits nonlinearity[6,7]. This nonlinearity would create a deviation in beat frequency of the FSI signal, and thus result in severe degradation of dynamic ranging accuracy. There exists several methods to remove the impact of frequency-swept nonlinearity[6-10], while they are aimed at enhancing the static positioning resolution and are not suitable for dynamic targets. In other words, these methods lack the immunity to the Doppler effect.

To simultaneously address the two problems in dynamic ranging, real-time models using the Kalman filter[11-13] were proposed. These models only adopt one triangular-modulated FSL, but they reach the best performance only when the dynamic OPD satisfies the state transition matrix. The main reason is because they assume the OPD varies in constant velocity[11], or constant

acceleration[12,13] between two consecutive sampling points. Another approach is using the output signal of an auxiliary Mach-Zehnder interferometer (MZI) as a sampling clock to trigger the data acquisition system[14], by which the frequency sweep nonlinearity can be corrected. However, this approach would lead to an uneven sampling clock, which requires a sophisticated phase-locked loop (PLL) to correct the signal distortion of the laser Doppler velocimeter (LDV). Similarly, using equispaced-phase-resampled, nonlinearity-corrected, and triangular-modulated dual-path FSI[15] can remove the Doppler effect, while this method requires constant target velocity during a sweep period, and only gives a single distance value per sweep.

In Ref.[16], we reported a dynamic FSI (DFSI) which achieves a measurement rate of 5 MHz under 2 kHz frequency sweep rate, and this DFSI enables the elimination of Doppler error by using one frequency-fixed interferometry (FFI). However, this DFSI is incapable of removing the frequency-sweep nonlinearity. Here, we propose a new DFSI ranging model, which consists of two measurement interferometers (FSI and FFI) and two auxiliary interferometers (AU1 and AU2). The AU1, with fixed *OPD*, can provide the information of the nonlinearity of FSL, and the FFI and AU2 with the assistance of acoustic-optical modulators (AOMs) can give the information of the Doppler effect. Based on the above information, we propose a new fusion signal processing method to remove the two kinds of ranging errors in FSI and recover the dynamic distance at each sampling point.

Fig.1 shows a basic FSI in MZI. For a static target at fixed-distance L, and an ideal FSL without frequency-sweep nonlinearity, the beat frequency f_B of the FSI signal is[15]

$$f_B = \frac{d\varphi(t)}{2\pi dt} = k\frac{2nL}{c},\qquad(1)$$

where $\varphi(t)$ is the phase of FSI signal, k is the sweep rate of FSL, n is the refractive index of air, and c is the speed of light in vacuum. By measuring f_B, L can be obtained as $f_B(c/2nk)$. However, when target moves and frequency-sweep nonlinearity exists, f_B in Eq.(1) becomes[13]

$$f_B(t) = \frac{d\varphi(t)}{2\pi dt} = \frac{2n}{c}[L'(t)f(t) + L(t)f'(t)],\qquad(2)$$

where $L'(t)$ and $f'(t)$ are the first-order time derivative of the dynamic distance $L(t)$ and the output light frequency $f(t)$ of FSL ($f(t) = f_{INI} + kt + e(t)$, where f_{INI} is the initial frequency and $e(t)$ is the frequency-sweep nonlinearity). Thus, using $f_B(t)$, the measured dynamic distance $L_M(t)$ can be expressed as

$$L_M(t) = \frac{c}{2nk}f_B(t) =$$

$$L(t) + \underbrace{\frac{f_{INI} + kt}{k}L'(t)}_{Doppler} + \underbrace{\frac{[e(t)L(t)]'}{k}}_{Nonlinearity},\qquad(3)$$

where the second term is the Doppler error[16] sensitive to target velocity $L'(t)$, and the third term is the nonlinearity error induced by nonlinearity $e(t)$. Both terms severely restrict the dynamic ranging accuracy and need to be eliminated.
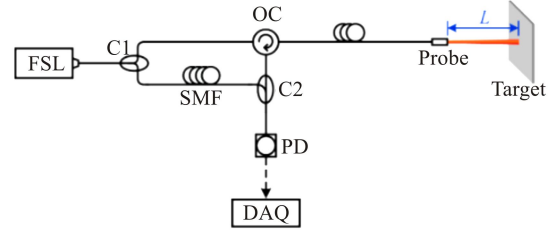
FSL: frequency-swept laser; C: coupler; SMF: single-mode fiber; OC: optical circulator; PD: photodetector; DAQ: data acquisition system

Fig.1 Schematic of basic FSI

To solve the above problems, a DFSI is proposed as shown in Fig.2. The laser source of AU1 and FSI is FSL, with their signals detected by photodetector 1 (PD1) and PD2, respectively. Similarly, the laser source of AU2 and FFI is FFL, with their signals respectively detected by PD3 and PD4. The wavelength division multiplexer (WDM) is used to separate the signals of FSI and FFI in the wavelength domain. The acoustic-optic modulators (AOM1 and AOM2) with a slight frequency difference are used to construct the heterodyne structures of AU2 and FFI. The combination of AU2 and FFI works as an LDV, used for monitoring the target displacement. Note that the dual-AOM configuration is also used to reduce the sampling rate of the data acquisition system (DAQ).
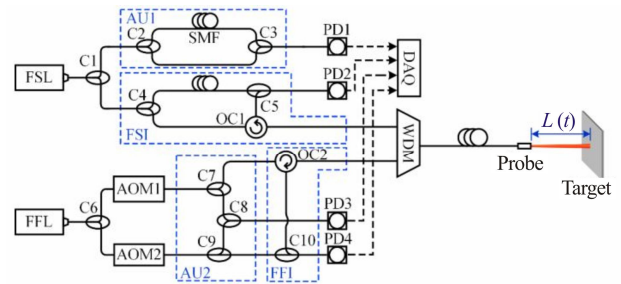
FSL: frequency-swept laser; FFL: frequency-fixed laser; C: coupler; SMF: single-mode fiber; OC: optical circulator; AOM: acoustic-optic modulator; WDM: wavelength division multiplexer; PD: photodetector; DAQ: data acquisition system

Fig.2 Schematic of the proposed DFSI

According to Eq.(2), the signal of the FSI is

$$s_{FSI}(t) = \cos\varphi_{FSI}(t) = \cos\left[2\pi\int_0^t f_B(t)dt\right] =$$

$$\cos\left\{\frac{4\pi n}{c}\left[k\int_0^t L(t)dt + \int_0^t (f_{INI} + kt)L'(t)dt + \right.\right.$$

$$\left.\left. e(t)L(t) + f_{INI}L(0)\right]\right\} =$$

$$\cos\left\{\frac{4\pi n}{c}\left[L(0)\int_0^t f'(t)\mathrm{d}t + \int_0^t f'(t)\mathrm{d}t\int_0^t L'(t)\mathrm{d}t + \right.\right.$$

$$\left.\left. f_{\mathrm{INI}}\int_0^t L'(t)\mathrm{d}t + f_{\mathrm{INI}}L(0)\right]\right\}, \tag{4}$$

where the last term $f_{\mathrm{INI}}L(0)(4\pi n/c)$ is a constant phase of $s_{\mathrm{FSI}}(t)$. After phase unwrapping, the incremental phase $\Delta\varphi_{\mathrm{FSI}}(t)$ of $s_{\mathrm{FSI}}(t)$ can be obtained as

$$\Delta\varphi_{\mathrm{FSI}}(t) = \frac{4\pi n}{c}\left[L(0)\int_0^t f'(t)\mathrm{d}t + \int_0^t f'(t)\mathrm{d}t\int_0^t L'(t)\mathrm{d}t + \right.$$

$$\left. f_{\mathrm{INI}}\int_0^t L'(t)\mathrm{d}t\right]. \tag{5}$$

Meanwhile, the signal of the AU1 can be expressed as

$$s_{\mathrm{AU1}}(t) = \cos\varphi_{\mathrm{AU1}}(t) =$$

$$\cos\left\{\frac{4\pi n_{\mathrm{F}}}{c}\left[L_{\mathrm{F}}\int_0^t f'(t)\mathrm{d}t + f_{\mathrm{INI}}L_{\mathrm{F}}\right]\right\}, \tag{6}$$

where n_{F} is the refractive index of single-mode fiber (SMF), and L_{F} is the fixed path-difference between two arms of AU1. Using phase unwrapping, the following equation can be obtained

$$\int_0^t f'(t)\mathrm{d}t = \frac{c}{4\pi n_{\mathrm{F}}L_{\mathrm{F}}}\Delta\varphi_{\mathrm{AU1}}(t), \tag{7}$$

where $\Delta\varphi_{\mathrm{FFI}}(t)$ is the incremental phase of $s_{\mathrm{AU1}}(t)$.

Similarly, the signals of FFI of AU2 respectively are

$$s_{\mathrm{FFI}}(t) = \cos\varphi_{\mathrm{FFI}}(t) =$$

$$\cos\left\{2\pi\int_0^t\left[\frac{2n(f_0+f_{\mathrm{AOM1}})L'(t)}{c}+\Delta f_{\mathrm{AOM}}\right]\mathrm{d}t\right\}, \tag{8}$$

and

$$s_{\mathrm{AU2}}(t) = \cos\varphi_{\mathrm{AU2}}(t) = \cos\left[2\pi\int_0^t \Delta f_{\mathrm{AOM}}\mathrm{d}t\right], \tag{9}$$

where f_0 is the light frequency of FFL, f_{AOM1} is the frequency shift of AOM1, and Δf_{AOM} is the frequency difference between AOM1 and AOM2. Using the incremental phases of $s_{\mathrm{FFI}}(t)$ and $s_{\mathrm{AU2}}(t)$, i.e., $\Delta\varphi_{\mathrm{FFI}}(t)$ and $\Delta\varphi_{\mathrm{AU2}}(t)$, the distance variation can be obtained as

$$\int_0^t L'(t)\mathrm{d}t = \frac{c\left[\Delta\varphi_{\mathrm{FFI}}(t)-\Delta\varphi_{\mathrm{AU2}}(t)\right]}{4\pi n(f_0+f_{\mathrm{AOM1}})}. \tag{10}$$

Then, substituting Eq.(7) and Eq.(10) into Eq.(5), we can construct a function $L_{\mathrm{c}}(f_{\mathrm{c}})$ as follows

$$L_{\mathrm{c}}(f_{\mathrm{c}}) = \frac{c\Delta\varphi_{\mathrm{FSI}} - \left[f_{\mathrm{c}}+\int_0^t f'(t)\mathrm{d}t\right]4\pi n\int_0^t L'(t)\mathrm{d}t}{4\pi n\int_0^t f'(t)\mathrm{d}t}, \tag{11}$$

where f_{c} is the constructed variable. Mathematically, the DFSI can be regarded as an underdetermined system with constraints, and when the variable $f_{\mathrm{c}}=f_{\mathrm{INI}}$, the $L_{\mathrm{c}}(f_{\mathrm{c}})$ becomes constant and equals $L(0)$. Such a condition can be found by the following function

$$f_{\mathrm{c\text{-}best}} = \underset{f_{\mathrm{c}}}{\arg\min}\left\{K = \mathrm{var}[L_{\mathrm{c}}(f_{\mathrm{c}})]\right\}. \tag{12}$$

When the $f_{\mathrm{c\text{-}best}}$ satisfying Eq.(12) is found, together with Eq.(10), the dynamic distance can be obtained as

$$L(t) = L_{\mathrm{c}}(f_{\mathrm{c\text{-}best}}) + \frac{c[\Delta\varphi_{\mathrm{FFI}}(t)-\Delta\varphi_{\mathrm{AU2}}(t)]}{4\pi n(f_0+f_{\mathrm{AOM1}})}. \tag{13}$$

It is worth noting that this method is not affected by the value of f_{INI}, in other words, besides the immunity to the Doppler effect and frequency-sweep nonlinearity, this method also has the immunity to the drift of f_{INI}.

Note that the measurable distance changing velocity is restrained by the following condition:

$$-kL_0 < \left[k\left(\int_0^t v(t)\mathrm{d}t\right)+(f_{\mathrm{INI}}+kt)v(t)\right] < \frac{c}{4n}f_{\mathrm{s}}-kL_0. \tag{14}$$

Numerical simulations were performed to verify the proposed DFSI. We assume the C-band FSL is with $f_{\mathrm{INI}}=$ 193 414 GHz (1 550 nm), k=3 000 GHz/s (bandwidth 300 GHz, sweep cycle 100 ms), and quadratic-form nonlinearity $e(t)$=$[8\times10^3\times(t-0.05)^2-20]$ GHz, and the O-band FFL is with f_0=228 849 GHz (1 310 nm), as shown in Fig.3(a). The target is set to vibrate with $L(t)=$ $[9.999\,9+1\times10^{-4}\cos(100\pi t)]$ m, as shown in Fig.3(b). The frequency shifts of AOM1 and AOM2 are assumed to be 42 MHz and 40 MHz, respectively, and we set c= 2.997 9$\times10^8$ m/s, n=1.000 27, $n_{\mathrm{F}}L_{\mathrm{F}}$=10 m, and sampling frequency of DAQ equals 10 MHz.

(a)

(b)
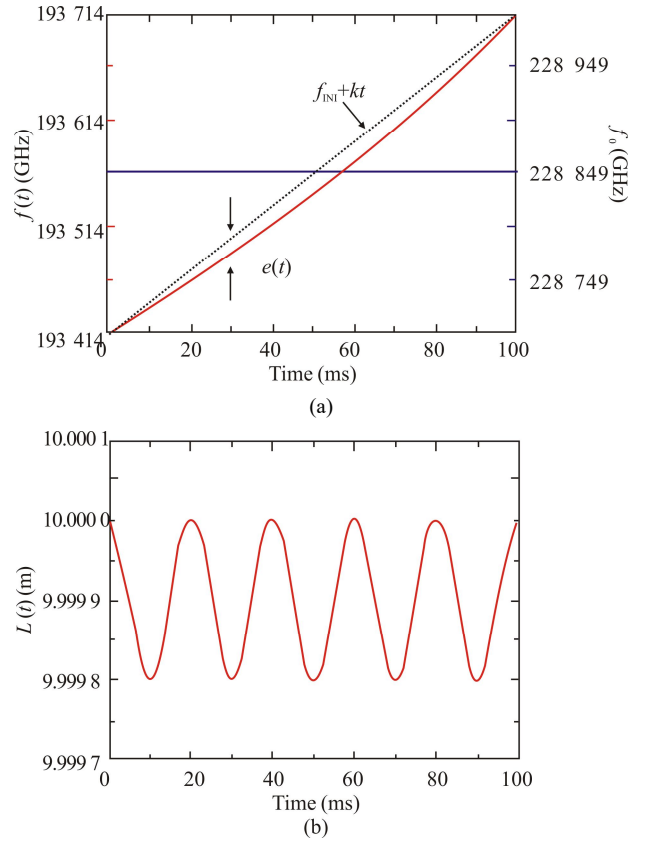
Fig.3 (a) Laser frequency $f(t)$ of FSL and f_0 of FFL; (b) Dynamic distance

To simulate the multiplicative and additive fluctuations caused by the variation of laser intensity[10] and the

random noise in practice, we contaminated the four interference signals by the form of $s_X(t)M(t)+A(t)+W(t)$, where $s_X(t)$ represents $s_{FSI}(t)$, $s_{FFI}(t)$, $s_{AU1}(t)$, or $s_{AU2}(t)$, $M(t)$ and $A(t)$ are the signal fluctuations, and $W(t)$ is the Gaussian noise. For the contaminated signals in Fig.3(a), the specific forms of $M(t)$, $A(t)$, and $W(t)$ of $s_X(t)$ are shown in Tab.1.

Tab.1 Specific forms of $M(t)$, $A(t)$ and $W(t)$

Signal	Form of $M(t)$	Form of $A(t)$	$W(t)$
$s_{FSI}(t)$	$0.5+2t$	$\sin(5\pi t)$	
$s_{FFI}(t)$	$0.5+2t$	$0.6\sin(5\pi t)$	White noise (20 dB)
$s_{AU1}(t)$	$0.6+4t$	$0.4\sin(5\pi t)$	
$s_{AU2}(t)$	$0.9+2t$	$\sin(8\pi t)$	

Before signal demodulation, the zero-phase band-pass filter is applied to each contaminated signal in Fig.4(a), and the filtered and normalized signals are shown in Fig.4(b). Then, the Hilbert transform (HT) method[10] is used to extract the corresponding incremental phase of each normalized signal. The incremental phases of FSI and AU1 are shown in Fig.4(c) and Fig.4(d), respectively. The incremental phase difference between the FFI and AU2 is shown in Fig.4(e). Fig.4(f) is the optimization space of f_c, and the optimized f_{c-best} is determined by positioning the minimum K, K_{min}. The theoretical optimization range of f_c is $(0, \infty)$, while it can be reduced by a priori knowledge of the output frequency of the FSL. Finally, according to the $K_{min}(f_{c-best})$, the dynamic distance at each sampling point can be recovered, as shown in Fig.4(g). The maximum error between the recovered $L_{Recover}(t)$ and the set $L(t)$ is about 0.350 μm.

To clearly show the feasibility of the proposed DFSI, for the same dynamic target, performance comparisons under two cases, (I) only the Doppler error existing and (II) both the Doppler error and nonlinearity error existing, are shown in Fig.5(a) and Fig.5(b), respectively. It can be seen that when the output laser frequency of FSL is linear ($e(t)=0$), for the dynamic target in Fig.3(b), the Doppler error contaminated distance $L_M(t)$ calculated by Eq.(3) and the distance $L_{Recover}(t)$ obtained by the proposed DFSI are plotted in Fig.5(a). It can be seen that the $L_M(t)$ contains the Doppler error which has a peak-to-peak amplitude of 9 477 955.8 μm as predicted by the theory, while the $L_{Recover}(t)$ given by DFSI eliminates the Doppler error and matches the $L(t)$ accurately, with the maximum error less than 0.363 μm. This indicates the proposed method works for removing the Doppler error. Then, for case (II) the same signal processing steps are applied, and the corresponding $L_M(t)$ and $L_{Recover}(t)$ are also plotted in Fig.5(b). It can be found that in this case, the $L_M(t)$ contains both the Doppler error ($f_{INI}+kt)L'(t)/k$ and nonlinearity error $[e(t)L(t)]'/k$, however, the $L_{Recover}(t)$ remains the accuracy as that in Fig.5(a). This

further demonstrates that the proposed DFSI has immunity to both the Doppler error and nonlinearity error.

(a)

(b)

(c)

(d)

(e)

(f)

(g)
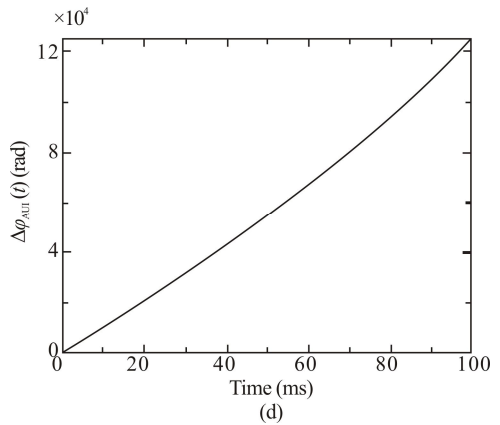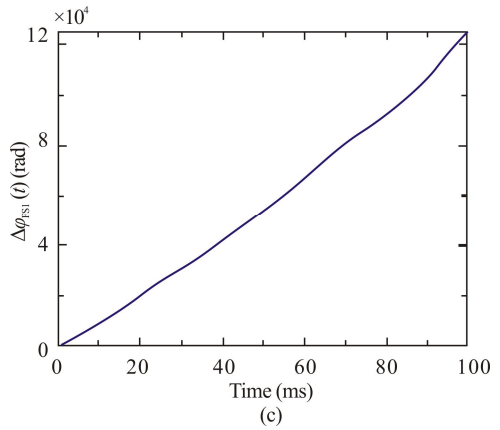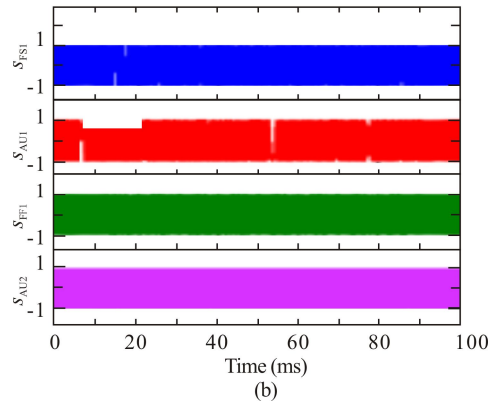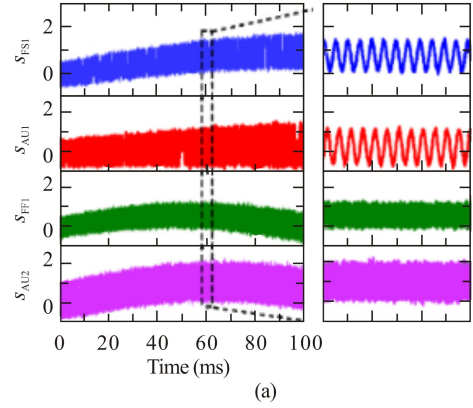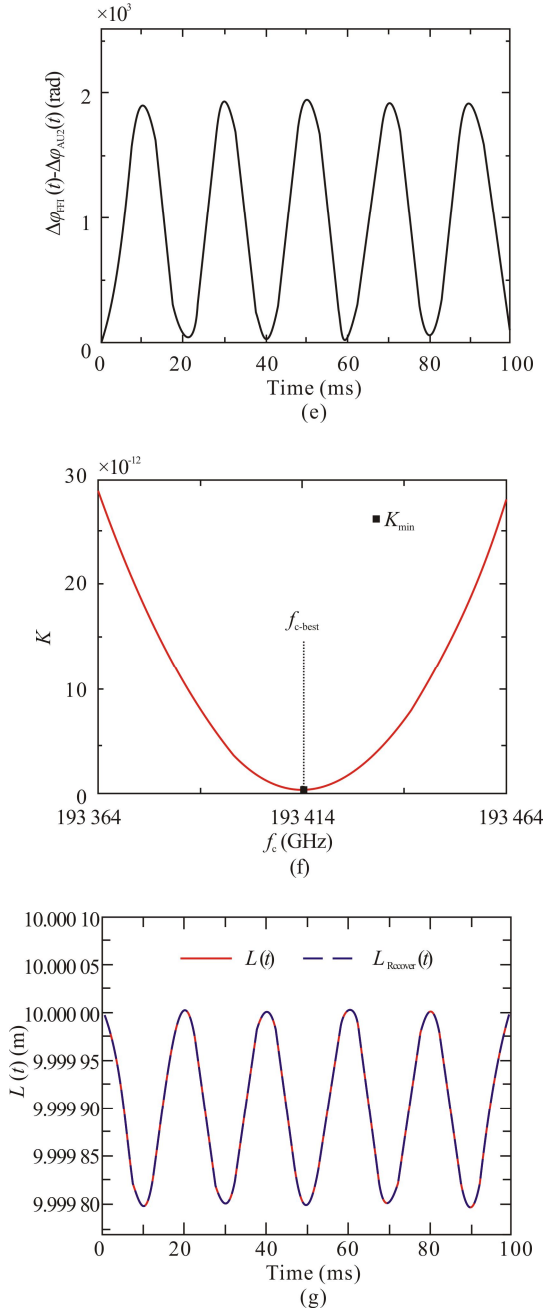
Fig.4 (a) Contaminated signals of $s_{FSI}(t)$, $s_{FFI}(t)$, $s_{AU1}(t)$, and $s_{AU2}(t)$; (b) Filtered and normalized $s_{FSI}(t)$, $s_{FFI}(t)$, $s_{AU1}(t)$, and $s_{AU2}(t)$; (c) Incremental phase of $s_{FSI}(t)$; (d) Incremental phase of $s_{AUI}(t)$; (e) Incremental phase difference between $s_{FFI}(t)$ and $s_{AU2}(t)$; (f) Optimization space of f_C; (g) Recovered dynamic distance $L_{Recover}(t)$ by the proposed method and the theoretical $L(t)$

This paper presents a novel DFSI that contains four interferometers, FSI, FFI, AU1, and AU2. By using their incremental phases, we construct a function to find the initial distance hidden in DFSI, and then eliminate the Doppler and nonlinearity errors, with the dynamic distance at each sampling point recovered. During measurement, the DFSI does not require prior information of

(a)

(b)
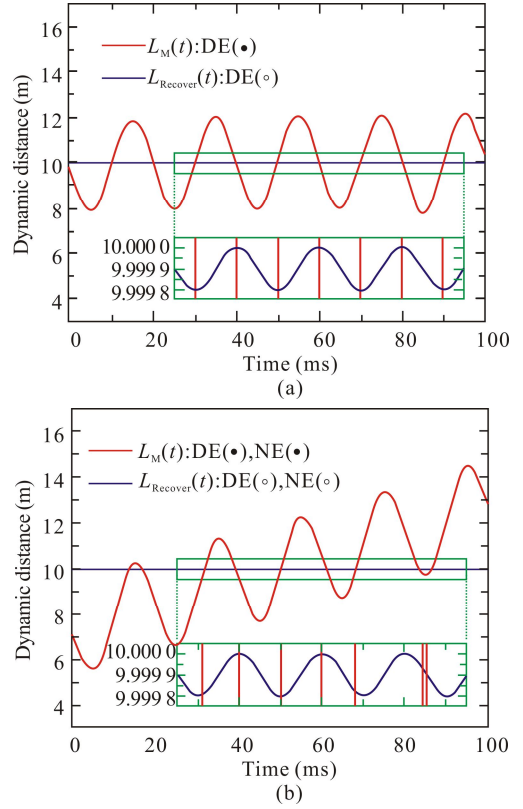
Fig.5 (a) Dynamic distance $L_M(t)$ recovered by Eq.(3) and $L_{Recover}(t)$ recovered by the proposed method in the case of FSL without frequency-sweep nonlinearity $e(t)$; (b) Dynamic distance $L_M(t)$ recovered by Eq.(3) and $L_{Recover}(t)$ recovered by the proposed method in the case of FSL with frequency-sweep nonlinearity $e(t)$. (DE(●): With Doppler error; DE(○): Without Doppler error; NE(●): With nonlinearity error; NE(○): Without nonlinearity error)

the FSL, and is not affected by the drift of the initial frequency of FSL. Moreover, the DFSI avoids the resampling process as reported in the previous works, and breaks the requirement of constant target velocity.

Statements and Declarations

The authors declare that there are no conflicts of interest related to this article.

References

[1] SHANG Y, LIN J R, YANG L H, et al. Precision improvement in frequency scanning interferometry based on suppression of the magnification effect[J]. Optics express, 2020, 28(4)：5822-5834.

[2] LIU H, ZHANG W, SHAO B, et al. Algorithm of Doppler error suppression in frequency-swept interferometry for the dynamic axial clearance measurement of high-speed rotating machinery[J]. Optics express, 2021, 29(26)：42471-42484.

[3]   SHAO B, ZHANG W, ZHANG P, et al. Multi-parameter measurement of rotors using the Doppler effect of frequency-swept interferometry[J]. Sensors, 2020, 20(24)：7178.

[4]   CHEN X L, WANG X C, PAN S L. Accuracy enhanced distance measurement system using double-sideband modulated frequency scanning interferometry[J]. Optical engineering, 2017, 56(3)：036114-036117.

[5]   CHEN Y, LEI X, XIAO L, et al. Dynamic distance measurement based on a fast frequency-swept interferometry[J]. Sensors, 2022, 22(13)：4771.

[6]   DENG Z, LIU Z, LI B, et al. Precision improvement in frequency-scanning interferometry based on suppressing nonlinear optical frequency sweeping[J]. Optical review, 2015, 22(5)：724-730.

[7]   ZHU Y, LIU Z G, DENG W, et al. Input signal shaping based on harmonic frequency response function for suppressing nonlinear optical frequency in frequency-scanning interferometry[J]. Review of scientific instruments, 2018, 89(5)：053109.

[8]   DENG W, LIU Z, DENG Z, et al. Extraction of interference phase in frequency-scanning interferometry based on empirical mode decomposition and Hilbert transform[J]. Applied optics, 2018, 57：2299-2305.

[9]   JIANG S, LIU B, WANG H, et al. Absolute distance measurement using frequency-scanning interferometry based on Hilbert phase subdivision[J]. Sensors, 2019, 19(23)：5132.

[10]   ZHU Y, WANG Z, TIAN K, et al. Phase-generated carrier combined with the Hilbert transform for phase demodulation in frequency-scanning interferometry[J]. Optics and lasers in engineering, 2022, 153：106988.

[11]   JIA X Y, LIU Z G, DENG Z W, et al. Dynamic absolute distance measurement by frequency sweeping interferometry based Doppler beat frequency tracking model[J]. Optics communications, 2019, 430：163-169.

[12]   JIA X, LIU Z, TAO L, et al. Frequency-scanning interferometry using a time-varying Kalman filter for dynamic tracking measurements[J]. Optics express, 2017, 25(21)：25782-25796.

[13]   DENG Z, LIU Z, JIA X, et al. Dynamic cascade-model-based frequency-scanning interferometry for real-time and rapid absolute optical ranging[J]. Optics express, 2019, 27(15)：21929-21945.

[14]   LU C, XIANG Y, GAN Y, et al. FSI-based non-cooperative target absolute distance measurement method using PLL correction for the influence of a nonlinear clock[J]. Optics letters, 2018, 43(9)：2098-2101.

[15]   ZHANG F, YI L, QU X. Simultaneous measurements of velocity and distance via a dual-path FMCW lidar system[J]. Optics communications, 2020, 474：126066.

[16]   SHAO B, ZHANG W, ZHANG P, et al. Dynamic clearance measurement using fiber-optic frequency-swept and frequency-fixed interferometry[J]. IEEE photonics technology letters, 2020, 32(20)：1331-1334.